Materials Science & Engineering A 766 (2019) 138371

Contents lists available at ScienceDirect

Materials Science & Engineering A

journal homepage: www.elsevier.com/locate/msea

Precipitation behavior and austenite stability of Nb or Nb–Mo micro-alloyed warm-rolled medium-Mn steels

Haijun Pan[a], Hua Ding[a,*], Minghui Cai[a], Dilay Kibaroglu[b], Yan Ma[b], Wenwen Song[b,**]

[a] School of Materials Science and Engineering, Northeastern University, Shenyang, 110819, China
[b] Steel Institute (IEHK), RWTH Aachen University, Intzestraße 1, 52072, Aachen, Germany

ARTICLE INFO

Keywords:
Medium-Mn steel
Warm rolling
Precipitation behavior
Nb/Mo addition
Retained austenite

ABSTRACT

Precipitation behavior and austenite stability of the warm-rolled medium-Mn steels with different Nb/Mo additions annealed at different temperatures were investigated. The Nb or Nb–Mo additions decrease the volume fraction of retained austenite, but increase its mechanical stability. The Mo addition to the Nb-bearing steels can lead to a higher density and smaller mean size of the precipitates because of the decreased interfacial energy and enhanced precipitation kinetics. The optimal precipitation temperature of the designed steels is about 600 °C. The Nb–Mo bearing steels exhibit a mixture of equiaxed and lamellar grain morphologies, and exceptional mechanical properties, *i.e.* the average products of ultimate tensile strength and total elongation (PSE) values of approx. 62 GPa %. An increase in yield strength of 300 MPa can result from grain refinement and precipitation hardening by Nb–Mo addition.

1. Introduction

Medium-Mn steel as a candidate in the advanced lightweight material class has gained widespread attention due to the excellent combination of high strength (≥1 GPa) and good ductility (≥30%) [1–6]. To further improve the mechanical properties of medium-Mn steel, an addition of microalloying elements has been recently aroused more and more attention [3–6]. He et al. [3] demonstrated that VC precipitates played a role in increasing the yield strength (YS) of ferrite by hindering the dislocation motion. Han et al. [4] reported that TiC precipitation in a 0.15 wt.-% Ti-added 5 wt.-% Mn steel suppressed the grain growth of austenite. Yan and Zou et al. [5,6] designed medium-Mn steels microalloyed with Cu in order to control the amount and stability of reversed austenite as well as to improve the mechanical properties. Some studies also pointed out the C content in austenite can be decreased by the addition of strong carbide formers, for instance, Nb, V, Ti *etc.* The addition of these elements significantly affects the microstructure evolution during heat treatment processes [7–10]. In addition, solute behaviour of microalloying elements and their precipitates have substantial effects on the microstructure and mechanical properties of TRIP steels through precipitation, phase transformation and grain refinement [7–9]. However, the exploration of microalloying treatment in medium-Mn steels is still very limited in the literature.

Recently, a combination of Mo and other microalloying elements have been proposed to control the dynamic precipitation and precipitate coarsening behaviors in micro-alloyed steels [7,11–13]. The carbon activity in austenite can be decreased with an addition of Mo, which can also increase the solubility of microalloying elements in austenite and facilitate the formation of finer precipitates in the ferrite [7,11]. The misfit strain of precipitates in ferrite can be decreased through Mo incorporation with Nb, thus reducing energetic barriers at the early stages of nucleation [12]. Additionally, the transformation kinetics of precipitates, ferrite and austenite can be modified by an addition of Mo [12]. Cai et al. [14] reported that YS and the ductility of the 6.5 wt.-% Mn steel can be enhanced with an addition of 0.22 wt.-% Mo and 0.05 wt.-% Nb. An addition of 0.19 wt.-% Mo and 0.11 wt.-% Ti in a 4.1 wt.-% Mn steel was reported to improve strength without loss of elongation [15]. However, compared with the investigation on an individual microalloy addition during thermomechanical processing, few studies have been reported on the precipitation behaviors of multiple microalloy additions. Moreover, the precipitation kinetics of steels with multiple microalloy additions is greatly different compared with that of steels with an individual microalloy addition [7,11–13].

In this work, a systematic study was conducted to investigate the influence of the microalloying addition on microstructure evolution during intercritical annealing and subsequent mechanical properties in the warm-rolled (WRed) medium-Mn steels. For the purpose of analysis, a comparison was made among the steels with no microalloying

* Corresponding author.
** Corresponding author.
E-mail addresses: dingh@smm.neu.edu.cn (H. Ding), wenwen.song@iehk.rwth-aachen.de (W. Song).

https://doi.org/10.1016/j.msea.2019.138371
Received 19 July 2019; Accepted 2 September 2019
Available online 04 September 2019
0921-5093/

Table 1
The chemical composition (wt.%) and the Ae_3 temperature (°C) of the experimental steels.

Steels	C	Mn	Al	N	Nb	Mo	Ae_3
6Mn	0.17	5.6	1.2	0.028	–	–	761
6MnNb	0.19	5.8	1.1	0.020	0.05	–	753
6MnNbMo	0.20	5.6	1.2	0.014	0.05	0.22	762

addition, a single Nb addition and multi-additions of Nb–Mo. In particular, the effects of microalloying additions on volume fraction of retained austenite ($V_{\gamma R}$), stability of retained austenite as well as the precipitation behaviors of the WRed medium-Mn steels annealed at different temperatures were discussed in details.

2. Materials and experimental procedures

The chemical compositions and the Ae_3 temperatures (calculated by Therm-Calc software) of the designed steels are shown in Table 1. The steels were prepared by induction melting, heated at 800 °C and subsequently warm rolled at the initial rolling temperature of 700 °C to strips of 1.5 mm in thickness with a total reduction of 95%. Then the WRed specimens were intercritically annealed at 550 °C, 600 °C, 650 °C and 700 °C for 30min using a small muffle furnace, followed by air cooling to room temperature.

The tensile test specimens were prepared parallel to the rolling direction with a gauge section of 25 mm × 6 mm, according to the ASTM E8/E8M standard. Uniaxial tensile testing was performed at room temperature at a strain rate of 5×10^{-3} s^{-1} by using SANSCMT-5000 machine.

Scanning Electron Microscope (SEM) analyses were carried out using a field-emission Supra SSX-550 microscope. SEM specimens were etched by 15% $NaHSO_3$ solution after standard mechanical polishing. The average grain sizes were measured using the linear intercept method (ASTM E−112), based on the SEM micrographs. Transmission Electron Microscope (TEM) analyses were carried out using an FEI Tecnai G^2 F20 microscope operating at 200 kV equipped with a nanometer probe energy-dispersive X-ray spectrometer (EDS). TEM specimens were electrolytically jet polished in a solution of 95% CH_3COOH and 5% $HClO_4$ at 18 °C. Standard TEM techniques were used to characterize the morphology, size distribution, and chemical compositions of precipitates. A statistical method was used to obtain the volume fraction and size of nano-precipitates [16], and at least 500 particles from TEM images were randomly chosen for the analysis.

APT measurements were conducted on a Local Electrode Atom Probe (LEAP 4000X HR, Cameca Instruments, Inc., Madison, WI, USA) system equipped with a reflectron for improved mass resolving power. Measurements were performed in the voltage pulsing mode with a pulse fraction of 15%. The base temperature was constant during the measurements, of approx. 60 K. The collected raw datasets were reconstructed into three-dimensional (3D) atomic maps and a precise decomposition process was conducted using the integrated visualization and analysis software (IVAS).

The volume fraction of austenite was determined by X-ray Diffraction (XRD, Rigaku, D/Max2250/PC) using a Cu-Kα radiation source (λ = 1.5405 Å), based on a direct comparison of the integrated intensities of all diffraction peaks [17]. The scanning range, speed and step size were 40–100°, 2° min^{-1} and 0.02°, respectively.

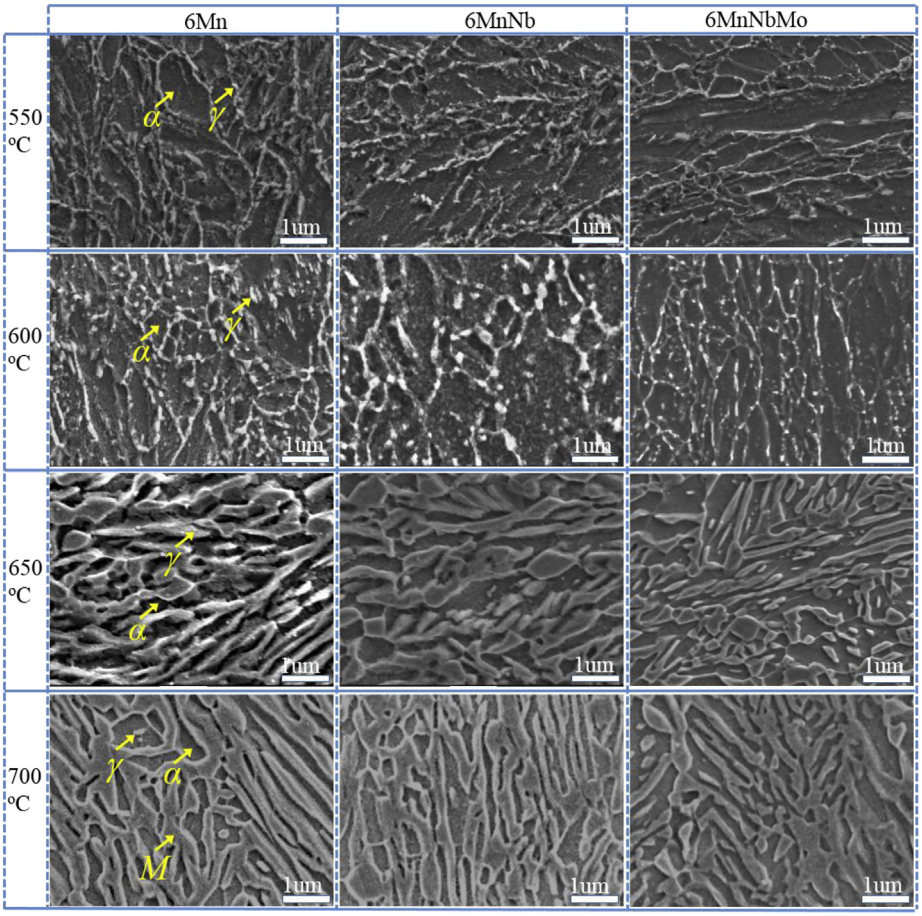

Fig. 1. The SEM micrographs of the WRed medium Mn steels 6Mn, 6MnNb and 6MnNbMo treated at 550 °C, 600 °C, 650 °C and 700 °C for 30min:γ-retained austenite, α-ferrite, M-martenite.

The dislocation density (ρ) was assessed by the following equation (1) [18]:

$$\rho = \frac{\beta^2}{4.35 \times b^2} \quad (1)$$

where $\beta$was the half-width of $(211)_\alpha$ diffraction peak and $b$was the burgers vector ($\sim 2.48 \times 10^{-8}$ cm).

3. Results

3.1. Microstructures

Fig. 1 presents the typical SEM microstructures of the investigated steels treated at 550 °C, 600 °C, 650 °C and 700 °C for 30 min. The microstructures of the annealed samples mainly comprised ferrite and retained austenite, which could be distinguished on the basis of their morphological features. An increase in the intercritical annealing (IA) temperature led to a decrease in the volume fraction of ferrite. In addition, martensite was found in the samples annealed at 700 °C, which is attributed to the insufficient thermal stability of austenite due to the low C/Mn contents and a large grain size of austenite. It should be noted that a mixture of lamellar and equiaxed grain morphologies were presented in all IAed samples, which may be caused by the insufficient driving force for active recrystallization of martensite of the WRed samples when the moderate rolling temperature was adopted [5,6]. In general, a raise in IA temperature results in an increase in mean grain size. Compared with the samples 6Mn, the addition of Nb and Nb–Mo greatly refined the mean grain size.

Fig. 2 displays the $V_{\gamma R}$ of the WRed samples as a function of the IA temperature. An increase in IA temperature from 550 °C to 650 °C led to the increase of $V_{\gamma R}$ from 5% to about 40%. Then $V_{\gamma R}$ decreases to about 30% with a further increase in IA temperature to 700 °C. It is noted that the addition of Nb, especially Nb–Mo co-addition, decreases the $V_{\gamma R}$ in the medium-Mn steels.

3.2. Mechanical properties

Fig. 3(a–c) shows the mechanical properties of the three steels intercritically annealed at different temperatures. The ultimate tensile strength (UTS) of the three steels increased with an increasing IA temperature up to 700 °C. The yield strength (YS) of the three steels manifested different responses to IA temperature. The YS of steel 6Mn continuously declined with an increase in IA temperature up to 700 °C. In contrast, the YS of steel 6MnNb and steel 6MnNbMo revealed minimal values when the IA temperature was 600 °C. IA temperature below 600 °C, YS showed a decrease trend with increasing IA temperature, while it increased with increasing IA temperature above 600 °C. The decreased YS may be due to an increase in average grain size with increasing IA temperature (Fig. 1). In contrast, the increase in YS of steel 6MnNb and steel 6MnNbMo annealed above 600 °C is believed to be associated with the enhanced precipitation behaviors (Fig. 4). Moreover, compared with steel 6Mn, the Nb and Nb–Mo increase the YS by 12–153 MPa and 88–301 MPa as well as the UTS by 15–139 MPa and 75–192 MPa respectively. The specific YS increment caused by the Nb or Nb–Mo additions at different IA temperatures is presented in Fig. 3(d), and the maximum (up to 301 MPa) is achieved at 600 °C. The Nb or Nb–Mo addition decreased the total elongation (EI) when the IA temperature was lower than 650 °C, but the EI exhibited an opposite trend in the materials annealed at a higher IA temperature (≥650 °C).

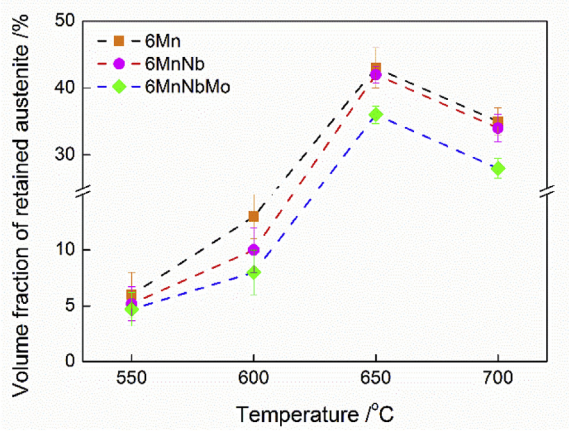

Fig. 2. The volume fraction of retained austenite of the WRed medium Mn steels 6Mn, 6MnNb and 6MnNbMo treated at 550 °C, 600 °C, 650 °C and 700 °C for 30min.

3.3. Precipitation characteristics

Fig. 4 presents the TEM results of the precipitates of the WRed Medium-Mn steels 6MnNb and 6MnNbMo at different IA temperatures. Lots of spherical precipitates were mainly distributed in the ferrite matrix, and the average size was less than 10 nm. Regardless of the single Nb or multiple Nb–Mo containing steels, the precipitate density reached the maximum at about 600 °C. The increase in IA temperature from 550 °C to 700 °C leads to about increase in the average precipitate size of 5 nm, as shown in Fig. 5. Moreover, the finer precipitates and the higher precipitate density can be achieved by the addition of Mo to the Nb-bearing steels.

3.4. Element distribution measured by APT

The APT micrographs of the precipitates are illustrated in Fig. 6 for the Nb and Nb–Mo bearing-steels annealed at 650 °C for 30min. The fine particles of the steels 6MnNb are identified as Nb(C,N) precipitates in Fig. 6(a), and the precipitates of the steels 6MnNbMo are identified as (Nb, Mo)(C,N) as shown in Fig. 6(b). In comparison to the Nb concentration in Nb(C,N), the Nb–Mo multiple addition drops the Nb concentration in (Nb, Mo)(C,N) up to 10 at.%.

To further characterize the element distribution influenced by the Nb or Nb–Mo addition, the one-dimensional concentration profile through the nano precipitates and neighboring matrix in three steels are shown in Fig. 6. The partitioning of C and Mn atoms to the austenite is clearly observed. Fig. 7 presents the C/Mn/Al concentrations (at.-%) in austenite and ferrite affected by the addition of Nb or Nb–Mo. The C and Al content (at.-%) of the steels with the Nb or Nb–Mo addition is higher than the ones in austenite of steels 6Mn. The addition of Nb and Nb–Mo increase the Mn and Al content (at. %) in ferrite.

4. Discussion

4.1. The mechanical stability of austenite affected by Nb/Mo additions

The mechanical stability of retained austenite is a key parameter to influence the mechanical properties of TRIP steels [19–24], which can be estimated by the stress-assisted martensitic transformation thermodynamic model [19,20]:

$$\Delta G^{chem} + \Delta G^{mech} > E^{store} \quad (3)$$

where, $\Delta G^{chem}$is chemical driving force for transformation, $\Delta G^{mech}$is the mechanical driving force, and $E^{store}$is the stored energy of martensite [19]. ΔG^{chem}can be calculated by equation (4) [24,25]:

$$\begin{aligned}\Delta G^{chem} = {} & x_c(16277 - 8.08T - 17660x_c - 10066x_{Mn}) \\ & + x_{Mn}(-430 + 0.305T) + x_{Mn}(1 - x_{Mn})(-6500 + 3.7T) \\ & + (1 - x_c - x_{Mn})\Delta G_{Fe}^{\gamma\rightarrow\alpha}\end{aligned} \quad (4)$$

Where x_c, x_{Mn}, $T$and $\Delta G_{Fe}^{\gamma\rightarrow\alpha}$are the mole fraction of C, the mole fraction

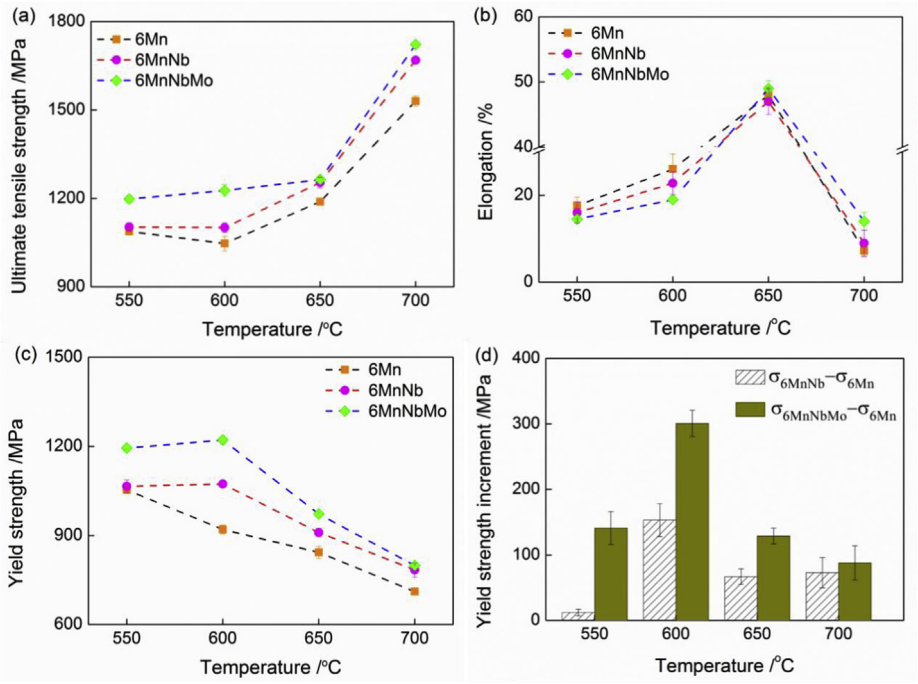

Fig. 3. Ultimate tensile strength (a), elongation (b), yield strength (c) and the increment of yield strength (d) of the WRed medium Mn steels 6Mn, 6MnNb and 6MnNbM treated at 550 °C, 600 °C, 650 °C and 700 °C for 30min: σ_{6Mn}-yield strength of steels 6Mn, σ_{6MnNb}-yield strength of steels 6MnNb and $\sigma_{6MnNbMo}$-yield strength of steels 6MnNbMo.

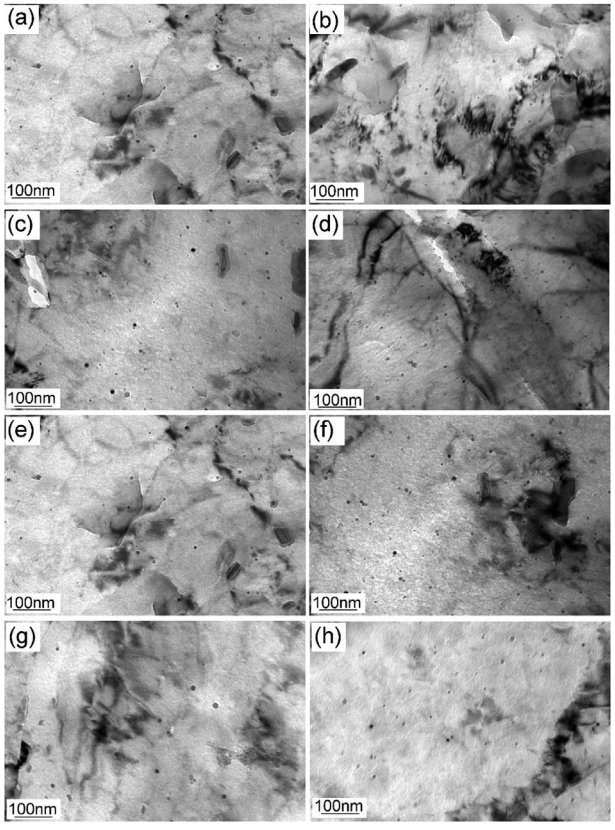

Fig. 4. The TEM micrographs of the precipitates of the WRed medium Mn steels 6MnNb (a, c, e, g) and 6MnNbMo (b, d, f, h) isothermally treated at 550 °C (a–b), 600 °C (c–d), 650 °C (e–f) and700 °C (g–h) for 30 min.

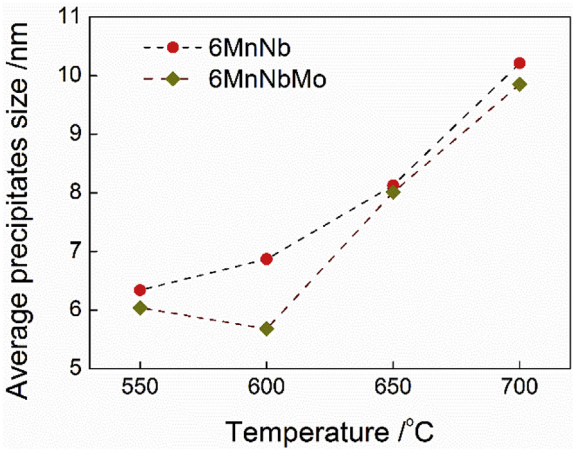

Fig. 5. Average precipitates size of the steels 6MnNb and 6MnNbMo annealed at various temperatures.

of Mn (Table 2), the temperature in Kelvin and the Gibbs free energy difference of the pure iron from austenite to ferrite respectively [24]. The increase in elastic strain energy per unit volume (ΔE_v) is given as [20]:

$$\Delta E_v = 1276.1(d_\gamma/\mathrm{d})^2 + 562.6(d_\gamma/d) \quad (5)$$

where, d_γ(Table 2) and d(about 0.4 μm based on the TEM) are the thickness of the austenite grain and the martensite plate respectively. Since the mechanical driving force can also be expressed as [19,20]:

$$\Delta G^{mech} = 0.86\sigma \quad (6)$$

Where, σ is the external stress, shown in Table 2. Compared with that of the steel 6Mn, the higher σ is necessary for the martensite transformation with the Nb or Nb–Mo addition, which mainly attributed to the smaller average grain size. Therefore, the Nb or Nb–Mo addition can increase the mechanical stability of retained austenite. As a result, the steels with a Nb addition, especially the Nb–Mo addition, can maintain

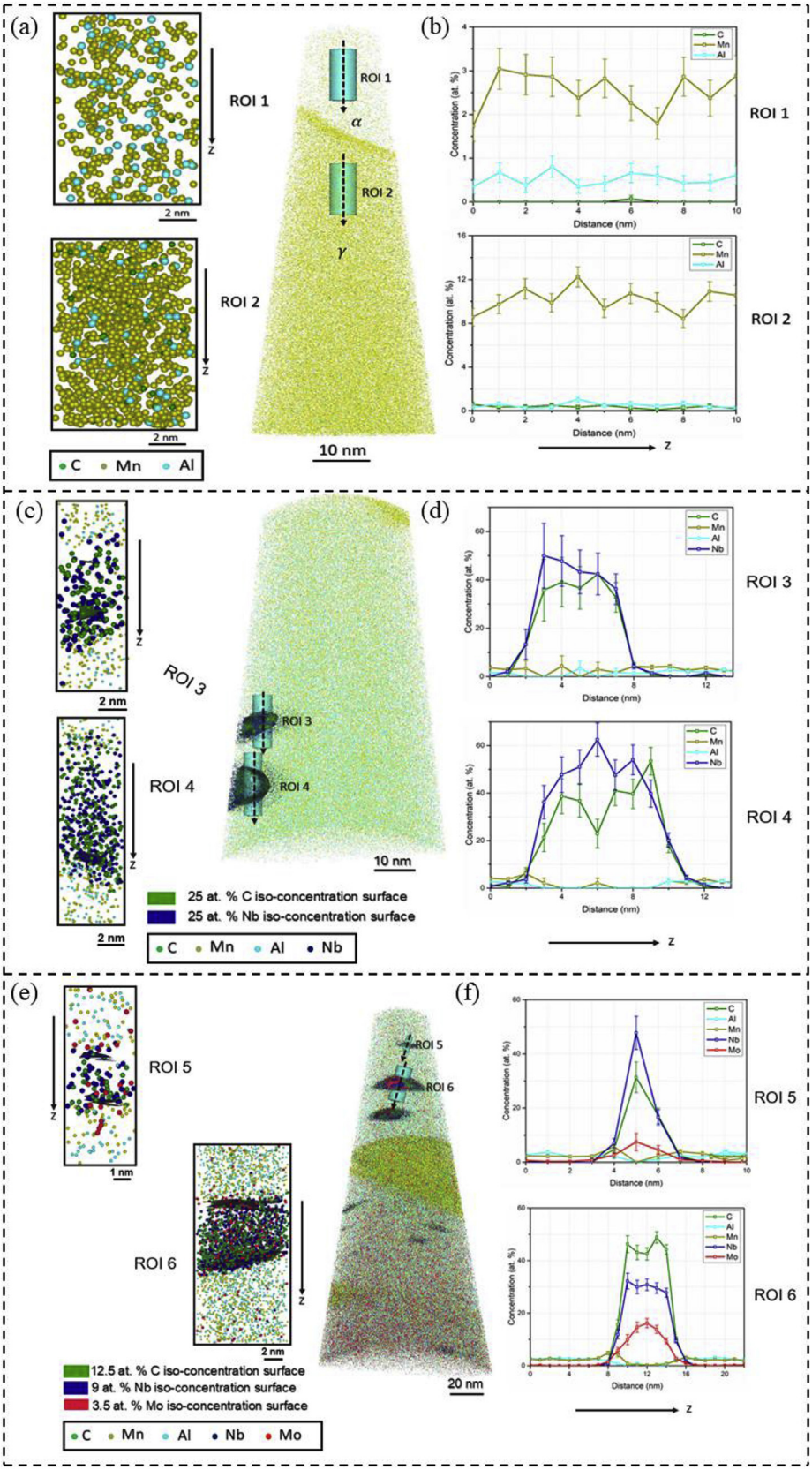

Fig. 6. APT characterization of the warm-rolled medium-Mn steels treated at 650 °C for 30 min. (a) Selected ROIs from austenite and ferrite phases in steel 6Mn. (c) Selected ROIs from carbides in steel 6MnNb. (e) Selected ROIs from carbides in steel 6MnNbMo. (b), (d) and (f) Concentration distribution plots obtained from the corresponding ROIs.

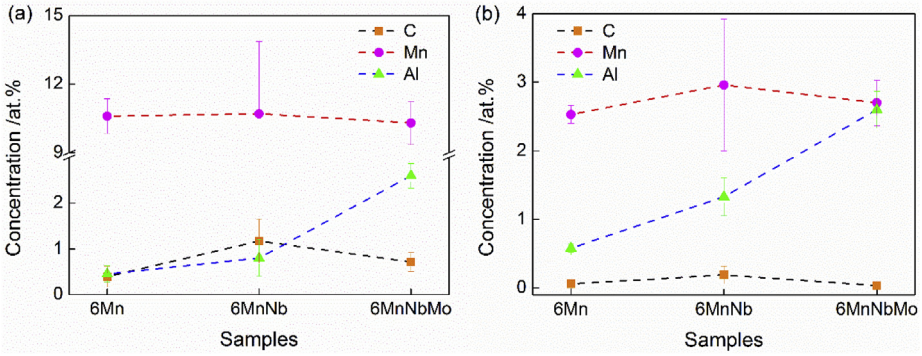

Fig. 7. The C, Mn and Al concentration (at.%) in austenite (a) and ferrite (b) of the warm rolled medium Mn steels treated at 650 °C for 30min.

Table 2
The C, Mn content in austenite, the mean austenite grain size (d_γ), the chemical driving force for martensite transformation (ΔG^{mech}), the increase in elastic strain energy per unit volume (ΔE_v) and the external stress (σ).

Steels	x_c/at.%	x_{Mn}/at.%	d_γ/um	ΔG^{chem}/(J/mol)	ΔE_v/(MJ/m^3)	σ/MPa
6Mn	0.39	10.6	0.20	1033.2	600.4	533.5
6MnNb	1.17	10.7	0.16	1111.1	850.1	811.5
6MnNbMo	0.71	10.3	0.15	1087.3	942.2	922.6

an excellent ductility with a relatively lower $V_{\gamma R}$.

4.2. The dependence of precipitation behavior and kinetics of (Nb_xMo_{1-x})(C, N) on the annealing temperature

As shown in Fig. 4, the composite precipitate phase (Nb_xMo_{1-x})(C,N) formed in the Nb–Mo bearing steels by the partial replacement of Nb by Mo [26], and the Mo/Nb atomic ratio in the (Nb_xMo_{1-x})(C, N) precipitates at different IA temperature is shown in Fig. 8(a). The star symbols represent the Mo/Nb atomic ratio in individual carbides and the square ones represent the average value of the Mo/Nb atomic ratio of the carbides. The maximum of Mo/Nb atomic ratio was achieved at IA temperature about 600 °C. Based on the semi-coherent interfacial misfit dislocation theory [26], the interfacial energy of (Nb_xMo_{1-x})(C, N) phase ($0.5 \le x \le 1$) in ferrite as a function of IA temperature can be calculated, as shown in Fig. 8(b). It was found that the replacement of Nb by Mo could reduce the interfacial energy, therefore the Mo addition to the Nb-bearing steel could benefit the higher density of precipitates [2,26–28].

According to Johnson-Mehl-Avrami equation, the precipitation-time-temperature (PTT) diagram can be calculated [26,27]. Assuming that the precipitation start time ($t_{0.05}$) is defined as the formation 5% of precipitate, and then the PTT diagram can be drawn basing on the results calculated as the following equation:

$$\lg\frac{t_{0.05}}{t_0} = \frac{1}{n}\left(-1.28994 - 2\lg d^* + \frac{1}{ln10} * \frac{\Delta G^* + \frac{5}{3}Q}{kT}\right) \quad (7)$$

Where, d^* is critical nucleation size, ΔG^* is critical nucleation energy,

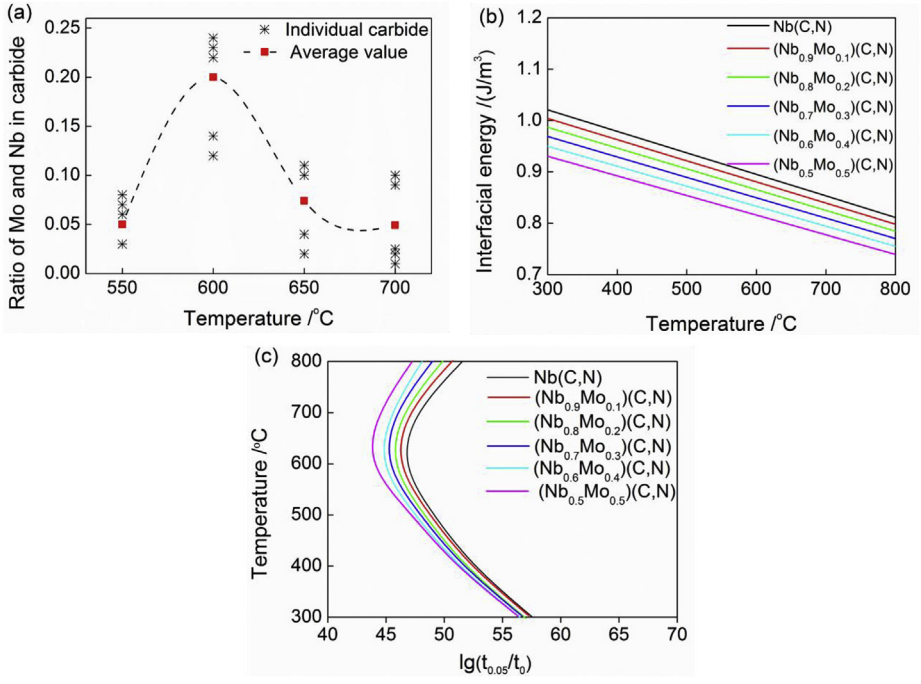

Fig. 8. The atomic ratio of Mo and Nb in carbides (a) and the interfacial energy between the (Nb_xMo_{1-x})(C,N) and ferrite (b) at different annealing temperature, and the precipitation-temperature-time (PTT) curves of (Nb_xMo_{1-x})(C,N) (c)($t_{0.05}$-the time when the precipitates mass fraction of (Nb_xMo_{1-x})(C,N) reaches 5%, t_0-constant irrelevant to time).

Table 3
The mean grain size (d), the total dislocation density (ρ_{total}), the average precipitates size (d^*) and the precipitation volume fraction of the WRed medium Mn steels 6Mn, 6MnNb and 6MnNbMo with different IA temperature.

Temperature/°C	$\bar{d}$/um			ρ_{total}/m^{-2}			d^*/nm			f		
	6Mn	6Mn Nb	6Mn NbMo	6Mn	6Mn Nb	6Mn NbMo	6Mn	6MnNb	6Mn NbMo	6Mn	6MnNb	6Mn NbMo
550	1.2	1.1	1.0	2.1×10^{14}	2.0×10^{14}	2.1×10^{14}	0	6.4	6.1	0	3.0×10^{-4}	5.1×10^{-4}
600	1.5	1.4	1.3	1.6×10^{14}	1.6×10^{14}	1.9×10^{14}	0	6.8	5.9	0	7.9×10^{-4}	12×10^{-4}
650	1.7	1.5	1.4	1.5×10^{14}	1.6×10^{14}	1.9×10^{14}	0	8.1	8.0	0	6.1×10^{-4}	10×10^{-4}
700	1.9	1.8	1.5	1.3×10^{13}	1.3×10^{13}	1.4×10^{13}	0	10.2	9.9	0	4.0×10^{-4}	7.1×10^{-4}

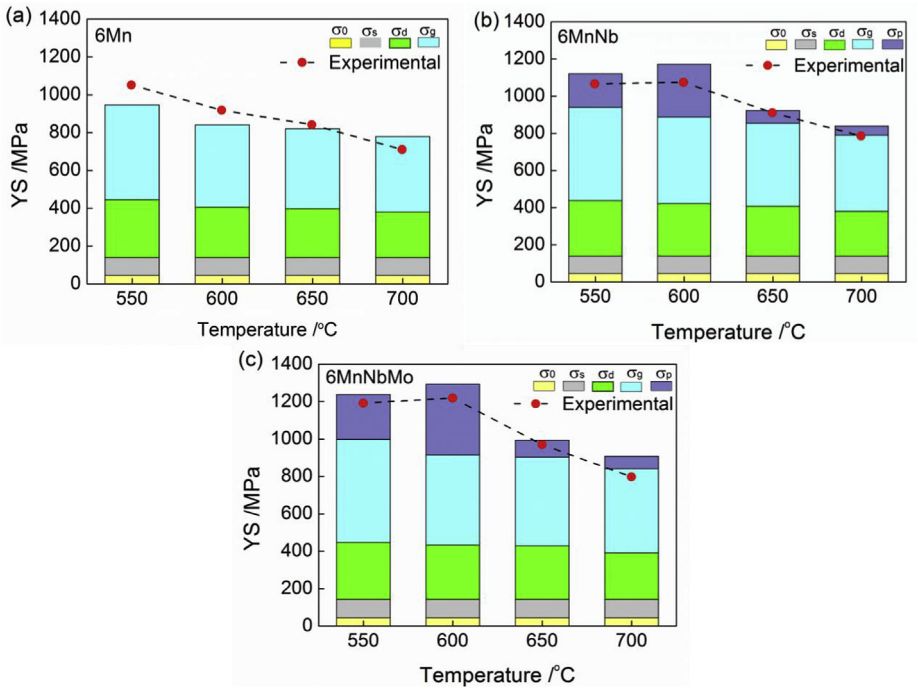

Fig. 9. The quantification of solid solution strengthening, grain refinement strengthening, dislocation hardening and precipitation hardening of the WRed medium Mn steels 6Mn (a), 6MnNb (b)and 6MnNbMo (c) at different IA temperature.

the time exponent n is approx. 1 [26]. The PPT diagram of (Nb_xMo_{1-x}) (C, N) phase in ferrite is shown in Fig. 8(c), which clearly indicates that the nose temperature was close to 600 °C. In addition, with the replacement of the Nb by Mo, the nose temperatures of the PPT curve move towards left upward, indicating that the replacement of Nb by Mo promotes the precipitation kinetics [28]. Besides, the Mo addition retards the coarsening of nano precipitates effectively [10]. Consequently, the Nb–Mo multiple addition increases the density of dispersed nano precipitates in ferrite. The result calculated by Avrami equation is in a good agreement with the experimental observations.

4.3. The quantification of the contribution to the YS with Nb or Nb–Mo addition

In order to obtain the quantitative assessment of the contributions to the YS with the addition of Nb or Nb–Mo, the YS (σ_y) was calculated by equation (8) [29]:

$$\sigma_y = \sigma_0 + \sigma_s + \sigma_g + \sigma_p + \sigma_d \quad (8)$$

He et al. pointed out that the initiation of yield point phenomenon in a medium-Mn steel occurred in the ferrite [30], thus the ferrite was mainly considered in calculation.

$\sigma_0$is the ferrite friction stress (~48 MPa [31]). σ_s, σ_g, $\sigma_p$and$\sigma_d$are the strengthening contribution caused by solid solution, grain refinement, precipitation hardening and dislocation hardening, respectively. The $\sigma_s$can be expressed using the empirical equation (9) [27]:

$$\sigma_s = 4570[C] + 4570[N] + 32[Mn] + 11[Mo] \quad (9)$$

where $[X_i]$ represents the mass percent of element X_i in ferrite and the value is calculated by the JmatPro. The $\sigma_g$can be calculated according to the Hall-Petch equation (10) [10]:

$$\sigma_g = k_y * d^{-0.5} \quad (10)$$

where $d$is the mean grain size (Table 3) and $k_y$is a constant (~17.4 $MPa/mm^{-0.5}$). For dislocation strengthening calculation, the Bailey-Hirsch relationship is used [31]:

$$\sigma_d = M\alpha Gb\sqrt{\rho_{total}} \quad (11)$$

here, $M$is the Taylor factor (~2.75 for random textured bcc metals [32]), $\alpha$is a constant (~0.38 in bcc iron [32]), $G$is the shear modulus (~81.6 GPa), $b$is the Burgers vector and ρ_{total}(Table 3) is the total dislocation density. Precipitation strengthening is given by the Ashby-

Orowan relation as follows [32]:

$$\sigma_p = \frac{9f^{0.5}}{d^*}\ln(1640d^*) \quad (12)$$

Where, f is the volume fraction of the precipitates and d^* is the average precipitate diameter (Table 3).

The calculated values for the different strengthening effects are shown in Fig. 9, which shows a relatively good agreement with the experimental results. It is clear that the Nb or Nb–Mo addition make a significant contribution to the YS mainly by the grain refinement and precipitation hardening, and the precipitation hardening makes a larger contribution to the YS than grain refinement.

5. Conclusions

In this paper, a systematic study of the effect of Nb or Nb–Mo microalloying addition on the fraction of austenite, stability of austenite and the precipitation behaviors of the WRed medium-Mn steels were conducted. The main conclusions are described as follows:

(1) The Nb or Nb–Mo addition increases the yield strength by 12–153 MPa or 88–301 MPa as well as the ultimate tensile strength by 15–139 MPa or 75–192 MPa compared with the steels without microalloying element addition. The maximum increment of the yield strength was achieved at intercritical annealing temperature about 600 °C.
(2) The Nb or Nb–Mo addition can reduce the fraction of austenite, but increase the mechanical stability of austenite by refining the mean grain size of austenite.
(3) The Mo addition can increase the precipitate density of $(Nb_xMo_{1-x})(C, N)$ by lowering the interfacial energy between the precipitates and matrix, and reduce the mean precipitate size, and the optimal precipitation temperature in this work was around 600 °C.
(4) The Nb or Nb–Mo addition increased the YS of the WRed medium-Mn steels mainly by the grain refinement and precipitation hardening, and the precipitation hardening makes a larger contribution to the YS than grain refinement.

Acknowledgements

The present work was financially supported by the National Natural Science Foundation of China (No. U1760205) and Henan Provincial Science and Technology Cooperation Project, China (No. 182106000016).

References

[1] J. Han, A.K.D. Silva, D. Ponge, D. Raabe, S.M. Lee, Y.K. Lee, S.I. Lee, B. Hwang, The effects of prior austenite grain boundaries and microstructural morphology on the impact toughness of intercritically annealed medium Mn steel, Acta Mater. 122 (2017) 199–206.
[2] H.J. Pan, M.H. Cai, H. Ding, H.S. Huang, B. Zhu, Y.L. Wang, Y.S. Zhang, Microstructure evolution and enhanced performance of a novel Nb-Mo microalloyed medium Mn alloy fabricated by low-temperature rolling and warm stamping, Mater. Des. 134 (2017) 352–360.
[3] B.B. He, B. Hu, H.W. Yen, G.J. Cheng, Z.K. Wang, H.W. Luo, M.X. Huang, High dislocation density-induced large ductility in deformed and partitioned steels, Science 357 (2017) 1029–1032.
[4] Y. Han, J. Shi, L. Xu, W.Q. Cao, H. Dong, TiC precipitation induced effect on microstructure and mechanical properties in low carbon medium manganese steel, Mater. Sci. Eng. A530 (2011) 643–651.
[5] S. Yan, T.S. Liang, J.Q. Chen, T.L. Li, X.H. Liu, A novel Cu-Ni added medium Mn steel: precipitation of Cu-rich particles and austenite reversed transformation occurring simultaneously during ART annealing, Mater. Sci. Eng. A 746 (2019) 73–81.
[6] P. Cheng, B. Hu, S.L. Liu, H. Guo, M. Enomoto, C.J. Shang, Influence of retained austenite and Cu precipitates on the mechanical properties of a cold-rolled and intercritically annealed medium Mn steel, Mater. Sci. Eng. A 746 (2019) 41–49.
[7] E. Abbasi, W.M. Rainforth, Microstructural evolution of Nb–V–Mo and V containing TRIP-assisted steels during thermomechanical processing, J. Mater. Sci. Technol. 33 (2017) 311–320.
[8] J. Kim, J.G. Jung, D.H. Kim, Y.K. Lee, The kinetics of Nb(C,N) precipitation during the isothermal austenite to ferrite transformation in a low-carbon Nb-microalloyed steel, Acta Mater. 61 (2013) 7437–7443.
[9] M. Kapoor, T. Kaub, K.A. Darling, B.L. Boycec, G.B. Thompson, An atom probe study on Nb solute partitioning and nanocrystalline grain stabilization in mechanically alloyed Cu-Nb, Acta Mater. 126 (2017) 564–575.
[10] H.J. Pan, H. Ding, M.H. Cai, Microstructural evolution and precipitation behavior of the warm-rolled medium Mn steels containing Nb or Nb-Mo during intercritical annealing, Mater. Sci. Eng. A 736 (2018) 375–382.
[11] C.M. Enloe, K.O. Findley, C.M. Parish, M.K. Miller, B.C. De-Cooman, J.G. Speer, Compositional evolution of microalloy carbonitrides in a Mo-bearing microalloyed steel, Scr. Mater. 68 (2013) 55–58.
[12] L. Jiang, R.K.W. Marceau, T. Dorin, P.D. Hodgson, N. Stanford, Effect of molybdenum on phase transformation and microstructural evolution of strip cast steels containing niobium, J. Mater. Sci. 54 (2019) 1769–1784.
[13] J.C. Cao, Q.L. Yong, Q.Y. Liu, X.J. Sun, Precipitation of MC phase and precipitation strengthening in hot rolled Nb-Mo and Nb-Ti steels, J. Mater. Sci. 42 (2007) 10080–10084.
[14] M.H. Cai, Z. Li, Q. Chao, P.D. Hodgson, A novel Mo and Nb microalloyed medium Mn TRIP steel with maximal ultimate strength and moderate ductility, Metall. Mater. Trans. A 45 (2014) 5624–5634.
[15] D. Lee, J.K. Kim, S. Lee, K. Lee, B.C.D. Cooman, Microstructures and mechanical properties of Ti and Mo micro-alloyed medium Mn steel, Mater. Sci. Eng. A 706 (2017) 1–14.
[16] X.Y. Sun, B. Zhang, H.Q. Lin, Y. Zhou, L. Sun, J.Q. Wang, E.H. Han, W. Ke, Correlations between stress corrosion cracking susceptibility and grain boundary microstructures for an Al–Zn–Mg alloy, Corros. Sci. 77 (2013) 103–112.
[17] N.H.V. Dijk, A.M. Butt, L. Zhao, J. Sietsma, S.E. Offerman, J.P. Wright, S.V.D. Zwaag, Thermal stability of retained austenite in TRIP steels studied by synchrotron X-ray diffraction during cooling, Acta Mater. 53 (2005) 5439–5447.
[18] C.G. Dunn, E.F. Kogh, Comparison of dislocation densities of primary and secondary recrystallization grains of Si-Fe, Acta Mater. 5 (1957) 548–554.
[19] H.W. Yen, S.W. Ooi, M. Eizadjou, A. Breen, C.Y. Huang, H.K.D.H. Bhadeshia, S.P. Ringer, Role of stress-assisted martensite in the design of strong ultrafine-grained duplex steels, Acta Mater. 82 (2015) 100–114.
[20] L.B. Luo, W. Li, L. Wang, S. Zhou, X.J. Jin, Tensile behaviors and deformation mechanism of a medium Mn-TRIP steel at different temperatures, Mater. Sci. Eng. A 682 (2017) 698–703.
[21] D.W. Suh, S.J. Kim, Medium Mn transformation-induced plasticity steels: recent progress and challenges, Scr. Mater. 126 (2017) 63–67.
[22] G. Olson, M. Cohen, Stress-assisted isothermal martensitic transformation: application to TRIP steels, Metall. Trans. A 13 (11) (1982) 1907–1914.
[23] O. Bouaziz, H. Zurob, M. Huang, Driving force and logic of development of advanced high strength steels for automotive applications, Steel Res. Int. 84 (10) (2013) 937–947.
[24] Z.Y. Xu, Martensitic Transformation and Martensite, Science Press, Beijing, 1999.
[25] K.N. Melton, O. Mercier, Fatique of NiTi thermoelastic martensite, Acta Metall. 27 (1979) 137–144.
[26] Q.L. Yong, Secondary Phase in Steels, Metallurgical Industry Press, Beijing, 2006.
[27] J.H. Jang, C.H. Lee, Y.U. Heo, D.W. Suh, Stability of (Ti, M)C (M = Nb, V, Mo and W) carbide in steels using first-principles calculations, Acta Mater. 60 (2012) 208–217.
[28] X.L. Li, Z.D. Wang, X.T. Deng, Y.M. Li, H.N. Lou, G.D. Wang, Precipitation behavior and kinetics in Nb-V-bearing low-carbon steel, Mater. Lett. 182 (2016) 6–9.
[29] D.B. Park, M.Y. Huh, J.H. Shim, J.Y. Suh, K.H. Lee, W.S. Jung, Strengthening mechanism of hot rolled Ti and Nb microalloyed HSLA steels containing Mo and W with various coiling temperature, Mater. Sci. Eng. A 560 (2013) 528–534.
[30] B.B. He, Z.Y. Liang, M.X. Huang, Nanoindentation investigation on the initiation of yield point phenomenon in a medium Mn steel, Scr. Mater. 158 (2018) 134–138.
[31] S.K. Ghosh, P.S. Bandyopadhyay, S. Kundu, S. Chatterjee, Copper bearing microalloyed ultrahigh strength steel on a pilot scale: microstructure and properties, Mater. Sci. Eng. A 528 (2011) 7887–7894.
[32] D.Y. Wu, X.L. Han, H.T. Tian, B. Liao, F.R. Xiao, Microstructural characterization and mechanical properties analysis of weld metals with two Ni contents during post-weld heat treatments, Metall. Mater. Trans. A 46 (2015) 1973–1984.